Kunkel, T. A. (1985a) *J. Biol. Chem. 260*, 5787–5796.
Kunkel, T. A. (1985b) *J. Biol. Chem. 260*, 12866–12874.
Kunkel, T. A. (1986) *J. Biol. Chem. 261*, 13581–13587.
Kunkel, T. A. & Alexander, P. S. (1986) *J. Biol. Chem. 261*, 160–166.
Kunkel, T. A., & Soni, A. (1988) *J. Biol. Chem. 263*, 4450–4459.
Kunkel, T. A., Gopinathan, K. P., Dube, D. K., Snow, E. T., & Loeb, L. A. (1986) *Proc. Natl. Acad. Sci. U.S.A. 84*, 1867–1871.
Kunkel, T. A., Sabatino, R. D., & Bambara, R. A. (1987) *Proc. Natl. Acad. Sci. U.S.A. 84*, 4865–4869.
Loeb, L. A., & Kunkel, T. A. (1982) *Annu. Rev. Biochem. 51*, 429–457.
Loeb, L. A., & Reyland, M. E. (1987) *Nucleic Acids Mol. Biol. 1*, 157–173.
McMahon, G., Davis, E., & Wogan, G. N. (1987) *Proc. Natl. Acad. Sci. U.S.A. 84*, 4974–4978.
Saiki, R. K., Scharf, S., Faloona, F., Mullis, K. B., Horn, G. T., Erlich, H. A., & Arnheim, N. (1985) *Science (Washington, D.C.) 230*, 1350–1354.
Saiki, R. K., Gelfand, D. H., Stoffel, S., Scharf, S. J., Higuchi, R., Horn, G. T., Mullis, K. B., & Erlich, H. A. (1988) *Science (Washington, D.C.) 239*, 487–491.

Deoxyribose Ring Conformation of $[d(GGTATACC)]_2$: An Analysis of Vicinal Proton–Proton Coupling Constants from Two-Dimensional Proton Nuclear Magnetic Resonance†

Ning Zhou,‡,§ Sadasivam Manogaran,‡,∥ Gerald Zon,⊥ and Thomas L. James*,‡

Departments of Pharmaceutical Chemistry and Radiology, University of California, San Francisco, California 94143, and Applied Biosystems, Foster City, California 94404

Received December 14, 1987; Revised Manuscript Received April 4, 1988

ABSTRACT: Exchangeable and nonexchangeable protons of $[d(GGTATACC)]_2$ in aqueous cacodylate solution were assigned from two-dimensional nuclear Overhausser effect (2D NOE) spectra. With phase-sensitive COSY and double quantum filtered COSY (DQF-COSY) experiments, the cross-peaks resulting from deoxyribose ring conformation sensitive proton–proton vicinal couplings, i.e., all 1′–2′, 1′–2″, 2′–3′, and 3′–4′ couplings and six from 2″–3′ couplings, were observed. From the cross-peak fine structure, the 2′,2″ proton assignments can be confirmed; coupling constants $J_{1'2'}$ and $J_{1'2''}$ and sums of coupling constants involving H2′ and H2″ for all residues and H3′ for C8 were obtained. The DISCO procedure [Kessler, H., Muller, A., & Oschkinat, H. (1985) *Magn. Reson. Chem. 23*, 844–852] was used to extract individual 1′–2′ and 1′–2″ coupling constants. The sum of coupling constants involving H1′ or H3′ was measured from the one-dimensional spectrum where signal overlap is not a problem. Analysis of the resulting coupling constants and sums of coupling constants, in the manner of Rinkel and Altona [Rinkel, L. J., & Altona, C. (1987) *J. Biomol. Struct. Dyn. 4*, 621–649], led to the following conclusion: C2′-endo deoxyribose ring conformation is predominant for every residue, but a significant amount of C3′-endo conformation may exist, ranging from 14% to 30%.

X-ray diffraction and NMR studies provide evidence (Saenger, 1984; Altona, 1982) that deoxyribose sugar rings in DNA molecules occur as two distinct types of conformers, commonly denoted as N-type [with the five membered ring pseudorotation phase angle (Altona & Sundaralingam, 1972) $P = 0 \pm 90°$, including C3′-endo, C2′-exo, and C4′-exo] and S-type (with $P = 180 \pm 90°$, including C2′-endo, C3′-exo, and C1′-exo). In B-DNA, sugar rings are generally in S-type conformation; in A-DNA, they are in N-type; and in Z-DNA, N and S conformers alternate. However, significant deviations from the above have been found in single-crystal X-ray diffraction studies.

The two types of sugar ring manifest quite different proton–proton coupling constants. From sugar exocyclic proton (H1′, H2′, H2″, H3′, and H4′) vicinal coupling constants, one can deduce pseudorotational parameters describing sugar ring conformation and relative populations of these conformers (de Leeuw & Altona, 1982, 1983). Various techniques have been developed to obtain these coupling constants from NMR experiments and to analyze them in terms of deoxyribose conformation. The conventional one-dimensional (1D) double-resonance method is not very useful when signal overlap is significant. Two-dimensional (2D) *J*-resolved and *J*-correlated spectra (COSY) and their 1D versions (Bermel et al., 1986; Kessler et al., 1987) provide more powerful ways to resolve proton multiplet structure. A pulse sequence has been suggested to obtain simplified cross-peak fine structure in a 2D correlated spectrum (exclusive COSY; Griesinger et al., 1985) to facilitate coupling constant determination. Kessler et al.

† This work was supported by the National Science Foundation (Grant PCM 84-04198), the National Institutes of Health (Grants CA 27343 and RR01695), donors of the Petroleum Research Fund, administered by the American Chemical Society, and instrumentation grants from the National Institutes of Health (RR 016688) and the National Science Foundation (DMB 84-06826).

* Address correspondence to this author at the School of Pharmacy, UCSF, San Francisco, CA 94143.
‡ University of California.
§ Present address: Department of Biological Sciences, University of Calgary, Calgary, Alberta, Canada T2N 1N4.
∥ Present address: Department of Chemistry, Indian Institute of Technology, Kampur, India 208 016.
⊥ Applied Biosystems.

0006-2960/88/0427-6013$01.50/0

(1985) proposed a procedure which they called DISCO, taking differences and sums of COSY subspectra, to simplify cross-peak structure and to extract individual coupling constants or sums and differences of coupling constants. Also, a COSY simulation program was developed (Widmer & Wüthrich, 1986, 1987) which may be used to determine coupling constants. A graphic method was suggested by Rinkel and Altona (1987) to analyze sugar conformation on the basis of easily determined coupling constants and sums of coupling constants. Use of these methods should enable one to gain insight into sugar ring conformation and conformational space in oligonucleotides.

Previous 2D NOE studies of $[d(GGTATACC)]_2$ from our group (Jamin et al., 1985; Zhou et al., 1987) revealed a B-type of structure for this duplex, with the middle -TATA- moiety more closely resembling a wrinkled-D structure (a subgroup of B-type DNA). To augment the information derived from 2D NOE studies, we conducted the present investigation. The motivation for these studies is an understanding of the structural basis for recognition in -TATA- sequences in the promoter region of genes. Questions to be examined include the following: is the deoxyribose sugar ring conformation in the -TATA- moiety correlated with the difference in backbone structure and are there any significant differences in conformational flexibility of the sugar rings in the -TATA- segment and in the GC parts. Phase-sensitive COSY spectra of the octamer duplex were obtained and analyzed to shed light on these questions.

Materials and Methods

The octanucleotide $[d(GGTATACC)]_2$ was synthesized by a solid-phase phosphoramidite method as described previously (Broido et al., 1984). Its purity was checked by HPLC, by base composition analysis, and by ^1H and ^{31}P NMR. The lyophilized sample was dissolved in a cacodylate buffer (10 mM cacodylate, 0.1 M NaCl, 0.5 mM EGTA, pH 7.0, 90% H_2O/10% D_2O) to give a concentration of 3 mM in duplex. This sample was used to obtain 2D NOE spectra of exchangeable and nonexchangeable protons. Then it was lyophilized several times from D_2O solution, and 99.996% D_2O (ICN Biomedicals) was finally added under dry nitrogen atmosphere for NMR experiments with nonexchangeable protons.

All ^1H NMR measurements were carried out at 20 °C on a 500-MHz spectrometer (General Electric GN-500) and processed with locally written software on a Vax 11/750 computer at the University of California, San Francisco. Double quantum filtered COSY (DQF-COSY) spectra were obtained with a time proportional phase incrementation scheme (Drobny et al., 1979; Bodenhausen et al., 1980; Marion & Wuthrich, 1983). The carrier frequency was set at the HDO peak frequency. Sweep width in both dimensions was 4540 Hz. In the phase-sensitive COSY experiment, 8K data points were collected and stored in alternate blocks, with 48 scans at each of 500 t_1 values. Apodization in both dimensions by a shifted sine-bell function before Fourier transformation, followed by zero-filling, resulted a final 4K × 1K data set. In the DQF-COSY experiment, 8K data point FID's were acquired with 48 scans at each of 860 t_1 values. Similar apodization functions were used. Zero filling once in the t_1 dimension gave a final data set of 4K × 1K size. Digital resolution was 1.1 Hz/point in ω_2 and 4.4 Hz/point in ω_1 for both experiments.

Phase-sensitive 2D NOE spectra were acquired as previously described (Jamin et al., 1985; States et al., 1982). A half-CYCLOPS phase cycling routine (Hoult & Richards, 1975; Stejskal & Shaefer, 1974) was applied in addition, resulting overall in 32-step phase cycling to suppress single and double quantum coherences as well as quadrature mismatch along ω_2 due to instrumental imperfections. A pulse repetition time of 3.5 s was used. The 2D NOE experiment in 90% H_2O/10% D_2O buffer solution was obtained with a $1\bar{3}\bar{1}$ excitation pulse (Hore, 1983) followed by a short homospoil pulse to suppress the water signal. Sweep width was 10 kHz, and proton excitation was centered at 10.5 ppm, halfway between the imino proton and amino-aromatic proton regions. FID's were processed as described above for COSY experiments; one zero filling in the t_1 dimension resulted a final 1K × 1K data set, with a resolution of 10 Hz/point in both dimensions.

COSY spectra were analyzed by the DISCO procedure of Kessler et al. (1985). The algebraic sum of a cross-peak or diagonal peak was obtained by adding or subtracting, according to the sign of the signals, the 2D COSY slices of this peak along the ω_2 dimension to improve S/N ratio. Typically, 10–12 slices from the well-resolved outer components of a cross-peak or from the diagonal peak were used to obtain a composite peak. The composite peaks were then used to generate the difference or summation spectra from corresponding peaks. When the operation involved a diagonal peak and a cross-peak, proper scaling was employed to achieve signal cancellation.

Results and Discussion

Assignment of Exchangeable and Nonexchangeable Proton Resonances. Cacodylate buffer solution was used for the NMR sample as a basis for future drug and protein binding studies and for the possibility of obtaining ^{31}P spectra with the same sample. The buffer salt resonances do not affect 2D spectral analysis of the octamer sample. There are some differences between the 500-MHz ^1H spectra of the octamer in neutral cacodylate buffer and phosphate buffer, in which assignments of nonexchangeable protons have been reported (Jamin et al., 1985), so phase-sensitive 2D NOE spectra in 90% H_2O/10% D_2O were used to obtain assignments for exchangeable protons as well as nonexchangeable protons. Most of the proton chemical shift differences between these two buffer solutions occurred at terminal residues. Nonexchangeable protons were assigned in a sequential manner (Hare et al., 1983; Scheek et al., 1983, 1984; Broido et al., 1984). Resulting assignments are given in Table I.

Imino proton assignments can be made from their sequential temperature broadening; the chemical shifts agree closely with assignments of Patel et al. (1986) for imino protons in phosphate buffer. At 20 °C and a mixing time of 200 ms, the G1 NH diagonal peak was not detected, but it exhibited a very broad exchange cross-peak with water (Figure 1A). G2 NH gave two cross-peaks to C^7 NH_2^d and NH_2^u; these two C7 amino protons are characterized by a strong cross-peak between them and by their NOE peaks to C7 H5 at 5.35 ppm (Figure 1A). G2 amino protons were tentatively assigned to the 6.83 ppm signal, which displays a weak cross-peak to G2 H1′. No NOE cross-peaks between G2 NH and NH_2 were properly resolved. The amino proton signals indicate slow exchange between the two C7 amino protons but probably fast exchange between the two G2 amino protons on the NMR chemical shift time scale; this observation is consistent with several cases of oligonucleotide C and G amino protons found by others (Boelens et al., 1985). The two C8 amino protons were assigned on the basis of their cross-peak to C8 H5 (5.71 ppm) and the cross-peak between them. No cross-peaks were detected between T NH and A NH_2 protons in one base pair. A4 and A6 amino protons were tentatively assigned to the 6.83 ppm

Table I: Chemical Shifts[a] of $[d(GGTATACC)]_2$ Protons

	G1	G2	T3	A4	T5	A6	C7	C8
H8	7.90	7.85		8.35		8.26		
H6			7.32		7.21		7.37	7.65
H5							5.35	5.71
H2				7.33		7.43		
CH3			1.47		1.47			
H1′	5.74	6.06	5.81	6.29	5.66	6.20	5.95	6.22
H2″	2.72	2.83	2.57	2.95	2.44	2.85	2.42	2.25
H2′	2.61	2.67	2.23	2.68	2.06	2.69	2.09	2.25
H3′	4.88	5.04	4.98	5.08	4.93	5.07	4.83	4.58
H4′	4.19	4.42	4.26	4.45	4.20	4.42	4.17	4.03
NH	12.60	12.79	13.39		13.27			
NH_2		(6.83)		(7.65)		(7.65)	6.64	6.99
NH_2				(6.83)		(6.83)	8.15	8.08

[a] Chemical shifts (ppm) are relative to sodium 3-(trimethylsilyl)[2,2,3,3-D_4]propionate at 20 °C. Parentheses are placed around tentative assignments.

Table II: Observed Coupling Constants and Sums and Differences of Coupling Constants (Hz) of $[d(GGTATACC)]_2$[a]

	$\sum 1'$					$\sum 2'$			$\sum 3'$	
residue	*b*	*c*	$\lvert J_{1'2'} - J_{1'2''}\rvert$	$J_{1'2'}$[d]	$J_{1'2''}$[e]	*c*	*g*	$\sum 2''$[c]	*b*	*h*
G1	13.9	14.4	≤2.8	8.8	5.5	27.0	29.0	22.5		
G2	13.3	14.4	≤3.1	8.3	6.1	28.0	28.0	23.5		
T3	14.0	14.4	≤3.1	8.8	5.5	29.0	30.0	23.0		
A4	14.7	15.6	≤3.1	8.9	6.7	28.0	30.0	24.0		
T5	14.8	14.4	≤3.0	8.8	5.5	28.9	28.5	22.0		
A6	14.0	14.4				28.9	30.0	22.5		
C7	13.7	13.3	≤2.0	7.8	5.5	29.0	30.0	23.5		
C8	13.9[e]	13.7				12.2[f]	12.2[f]		15.5	14.5

[a] The sums of coupling constants are as follows: $\sum 1' = J_{1'2'} + J_{1'2''}$, $\sum 2' = J_{1'}J_{2'} + J_{2'3'} + J_{2'2''}$, $\sum 2'' = J_{1'2''} + J_{2''3'} + J_{2'2''}$, and $\sum 3' = J_{2'3'} + J_{2''3'} + J_{3'4'}$. [b] First-order measurement from resolution-enhanced 1D spectrum; accuracy, ±0.6 Hz. [c] Measured from COY H1′–H2′,H2″ cross-peak splittings; accuracy, ±1.1 Hz. [d] Measured from DISCO spectra, see text for details. [e] Overlap, less accurate. [f] H2′ and H2″ of C8 are isochronous. [g] Measured from COSY H3′–H2′ cross-peak splittings; accuracy, ±1.1 Hz. [h] Measured from COSY H3′–H4′ cross-peak splittings; accuracy, ±1.1 Hz.

(more than two protons) and to the 7.65 ppm signals. Two medium-strong NOE peaks were detected between the base-paired T3 NH and A6 H2 and between T5 NH and A4 H2. These permitted assignment of the two adenine H2 protons, which were also consistent with detected cross-peaks of these H2 protons with other nonexchangeable protons.

It is interesting to note that two medium-strong cross-peaks were detected between each of the adenine H2 protons and the water protons (Figure 1), the cross-peak with A4 being narrower than that with A6. Possible explanations for these are (a) water molecules in the minor groove (Drew & Dickerson, 1981; Suzuki et al., 1986), which could be in close proximity to A H2, giving rise to this NOE interaction, (b) chemical exchange between T NH in the same base pair and water protons resulting in indirect exchange of A H2 and water proton magnetization, or (c) both. Cross-peaks in the 2D NOE experiment between A H2 and water proton resonances have also been observed for other oligomers (Kerwood, Suzuki, Laplanche, Scheek, and James, unpublished data).

Determination of Coupling Constants. Vicinal scalar coupling constants of deoxyribose ring protons in $[(GGTATACC)]_2$ were determined by phase-sensitive COSY and DQF-COSY experiments. The phase-sensitive COSY experiment provides the possibility to analyze both cross-peak and diagonal peak splitting patterns by utilization of DISCO processing and affords better S/N ratio than DQF-COSY. But the dispersion nature of the diagonal peaks makes observation of cross-peaks close to the diagonal difficult. In DQF-COSY, detection and pattern analysis of cross-peaks in regions close to the diagonal, for example, H3′ to H4′ and H2″ to H2′ regions, were easier.

Shown in Figure 2 is the COSY H1′–H2′,2″ cross-peak region, together with the 1D H1′ region. Every cross-peak is resolved. The upfield sugar H2′,2″ proton invariably (except in C8 where H2′ and H2″ are almost isochronous) shows a smaller passive coupling and a larger active coupling than the downfield one and can be assigned to H2′ which is trans to H1′. These assignments agree with previous results (Jamin et al., 1985). A cross-section of G1 H1′–H2′ and H1′–H2″ cross-peaks (Figure 3, panels I) illustrates the passive (in-phase) and active (antiphase) couplings more clearly. The H2′ and H2″ proton pair of G1 has the smallest chemical shift difference (except C8), 50 Hz, with a $\Delta\delta/J$ ratio of 3.6 (assuming an average geminal coupling constant $J_{2'2''} = 14$ Hz). According to Rinkel and Altona's (1987) simulation study, the distance between outer peaks of an H1′ signal is not affected by $\Delta\delta$ of H2′ and H2″ and is equal to $J_{1'2'} + J_{1'2''}$, and in cases with $\Delta\delta/J$ of H2′ and H2″ larger than 1.5, the individual vicinal coupling constants can be safely obtained by first-order measurement from the H1′ signal. But from the cross sections shown in Figure 3, it is clear that partial cancellation of the inner peaks occurs, resulting in smaller peaks; therefore direct first-order measurement of $J_{1'2'}$ and $J_{1'2''}$ at this line width cannot be obtained. On the other hand, the very slight overlap of outer and inner peaks in the H1′–H2′ cross-peak and slight cancellation of outer and inner peaks in the H1′–H2″ cross-peak apparently did not alter the outer-peak position, since the distances between outer peaks measured from the two cross-peaks agreed with each other within digital resolution; therefore, the outer-peak splitting manifests $J_{1'2'} + J_{1'2''}$. This was found for all seven residues. The summations of coupling constants ($\sum 1' = J_{1'2'} + J_{1'2''}$) for H1′ measured in this manner are listed in Table II. In the 1D spectrum, A6 H1′ and C8 H1′ peaks overlap, C8 H5 partially overlaps with G1 H1′, but peak overlap is far less a problem than in the H_2',H2″ region. H1′ outer-peak splittings were also measured from the 1D spectrum and are listed in Table II.

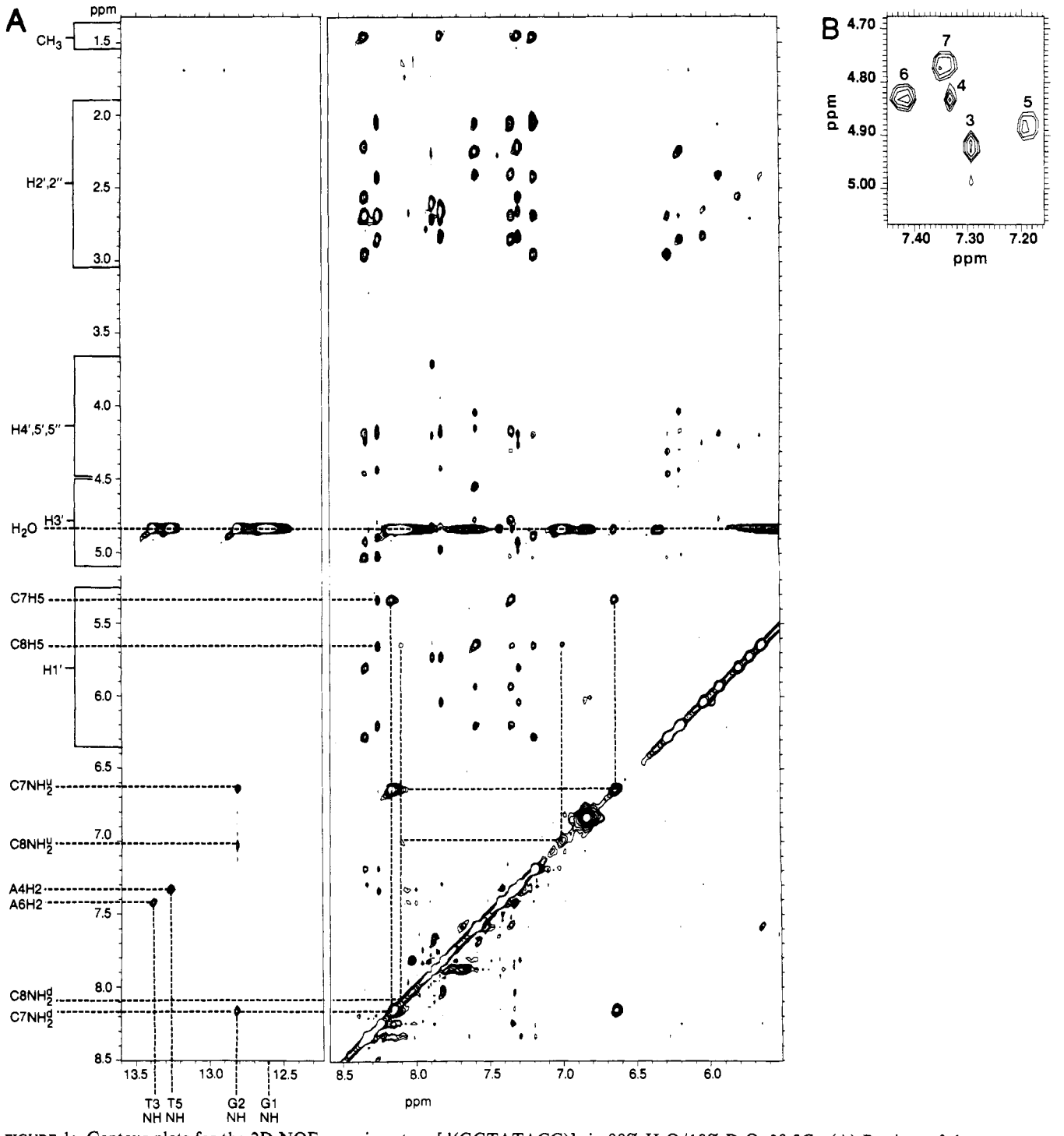

FIGURE 1: Contour plots for the 2D NOE experiment on $[d(GGTATACC)]_2$ in 90% H_2O/10% D_2O, 20 °C. (A) Portions of the spectrum downfield from the water signal. Some resonance of the exchangeable protons and the H2 protons of A4 and A6 are labeled. (B) An expanded spectral region showing cross-peaks between A4 H2 and water protons (labeled 4) and between A6 H2 and water protons (labeled 6). Cross-peaks labeled 3, 5, and 7 result from H3′–H6 interactions in T3, T5, and C7, respectively.

In order to obtain individual $J_{1'2'}$ and $J_{1'2''}$ coupling constants from phase-sensitive COSY data, the DISCO procedure (Kessler et al., 1985) was used (see Materials and Methods for details). Illustrated in Figure 4 as two examples are so-called decoupled DISCO spectra for H1′ of residues T3 and T5. In the frames labeled I and III, trace 1 is the algebraic sum of the outer components, i.e., composite peak (cf. Materials and Methods), of the H1′–H2′ cross-peak and trace 2 represents the composite H1′ diagonal peak. Since the H1′–H2′ cross-peak manifests in-phase H1′–H2″ splting and antiphase H1′–H2′ splitting, summation and subtraction of these two (1 + 2 and 1 − 2) gave two traces [marked as (+) and (−) in Figure 4] each of which exhibits splitting due to $J_{1'2''}$; the (+) and (−) traces are antiphase and shifted by a frequency of $J_{1'2'}$ with respect to each other. Values of $J_{1'2''}$ = 5.5 Hz and $J_{1'2'}$ = 8.8 Hz were obtained for T3 from direct measurement. Similarly, by use of the H1′–H2″ cross-peak and H1′ diagonal peak (Figure 4, frames II and IV), the $J_{1'2'}$ value can be measured from the resulting doublet splitting and $J_{1'2''}$ from the shift between the two doublets, providing a check for these values.

The measured $J_{1'2'}$ and $J_{1'2''}$ values are similar for all residues, i.e., coupling constant differences $|J_{1'2'} - J_{1'2''}|$ are small (≤3.1 Hz) for all residues. This results in an H1′ signal which

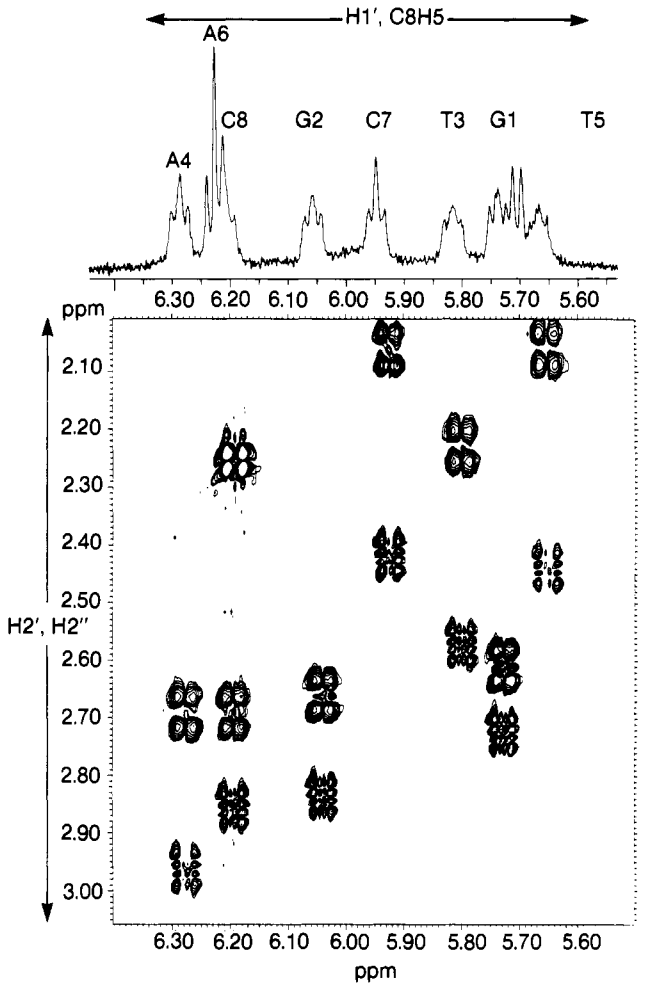

FIGURE 2: Contour plot of the H1′–H2′,H2″ cross-peak region of the $[d(GGTATACC)]_2$ phase-sensitive COSY experiment. At the top is a resolution-enhanced 1D spectrum of the H1′ region plotted along the ω_2 dimension of the contour plot. Assignments of H1′ protons are indicated. The doublet centered at 5.71 ppm is the C8 H5 signal.

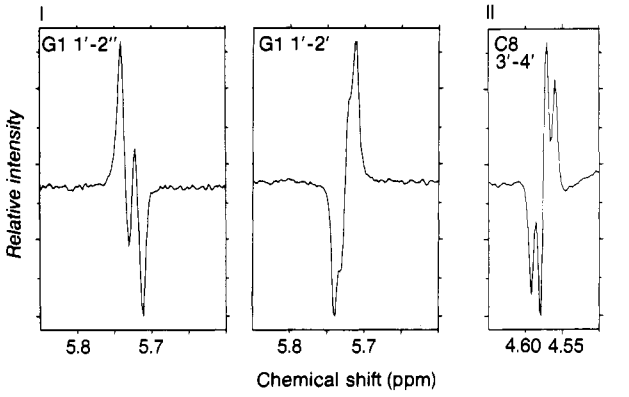

FIGURE 3: Slices from the phase-sensitive COSY experiment with $[d(GGTATACC)]_2$. The slices cut across the G1 H1′–H2′ and H1′–H2″ cross-peaks (I) and C8 H3′–H4′ cross-peak (II) along the ω_2 dimension. The intensity scale for the three slices is not identical.

appears to be a triplet (see Figure 2). In principle, $J_{1'2'} + J_{1'2''}$ and $|J_{1'2'} - J_{1'2''}|$ can be obtained from sums of H1′–H2′ and H1′–H2″ cross-peaks and from the difference between them (Kessler et al., 1985); therefore, the individual $J_{1'2'}$ and $J_{1'2''}$ values could be obtained. But when the $|J_{1'2'} - J_{1'2''}|$ values are no larger than half of the line width, severe overlap of the antiphase components prevents measurement of $|J_{1'2'} - J_{1'2''}|$ from the difference spectrum of the corresponding cross-peaks (or from each cross-peak), so only an upper limit on $|J_{1'2'} - J_{1'2''}|$ can be obtained. DISCO spectra between diagonal peaks and cross-peaks are superior for obtaining individual $J_{1'2'}$ and $J_{1'2''}$ values, since the resulting decoupled spectrum does not have antiphase components (Figure 4) and the coupling constants can be measured from the shift of the two decoupled spectra; therefore, coupling constants smaller than the line width can be extracted. When H1′ diagonal peaks partially overlap, correct coupling constants can still be determined from the nonoverlapping half. Individual $J_{1'2'}$ and $J_{1'2''}$ values for six residues, except A6 and C8 whose diagonal peaks overlap, are listed in Table II. The H2′,H2″–H1′ and H2′,H2″–H3′ cross-peak regions of the COSY contour spectrum are presented in Figure 5. Rinkel and Altona's (1987) simulation study found that the sums of proton–proton coupling constants to H2′ ($\sum 2' = J_{1'2'} + J_{2'3'} + J_{2'2''}$) and H2″ ($\sum 2'' = J_{1'2''} + J_{3'2''} + J_{2'2''}$) can be accurately determined by first-order measurement from the outer components of the cross-peaks in Figure 5 (A and B) when $\Delta\delta_{2'2''}/J_{2'2''} > 10$; the experimental error (<0.2 Hz) incurred by performing this measurement for $\sum 2'$ and $\sum 2''$ when $\Delta\delta_{2'2''}/J_{2'2''} > 2.9$ is easily within our digital resolution. Composite H2′–H1′ and H2′–H3′ cross-peaks (see Materials and Methods) were obtained to improve S/N, and $\sum 2'$ was measured from the outer components of the cross-peaks. Due to complicated and poorly resolved cross-peak fine structure along H2′, the position of the outer peak was often difficult to determine accurately; estimation of $\sum 2'$ was obtained from H2′–H1′ and H2′–H3′ cross-peaks, and values are listed in Table II.

One feature of the H2′,H2″–H3′ cross-peak region of the COSY contour spectrum (Figure 5B) is that, of the seven residues in which H2′ and H2″ resonances do not overlap, six H2″–H3′ cross-peaks were detected. They are weak or very weak, indicating small $J_{2''3'}$ since COSY cross-peak intensity is related to antiphase coherence transfer and its buildup rate is proportional to the active J value (Oschkinat & Freeman, 1984). The H2″–H3′ cross-peaks of T3 and A4 were barely detected, and that of T5 was not detected. The $\sum 2''$ values were determined from composite H2″–H1′ cross-peaks similar to the $\sum 2'$ measurements; values are given in Table II.

The last two columns in Table II are H3′ coupling constant sums, $\sum 3'$ ($=J_{2'3'} + J_{2''3'} + J_{3'4'}$), for C8 H3′. The coupling constant sum was measured from signal splitting in the 1D spectrum and from the outer component separation of the H3′–H4′ COSY cross-peaks (Figure 3, panel II), in a manner similar to the $\sum 2'$ measurement.

Deoxyribose Ring Conformation in the Octamer. A complete analysis of deoxyribose ring conformation entails measurement of five ^1H–^1H vicinal coupling constants ($J_{1'2'}$, $J_{1'2''}$, $J_{2'3'}$, $J_{2''3'}$, and $J_{3'4'}$). Considering experimental errors, more measurements at different temperatures and measurement of heteronuclear coupling constants would be desirable to improve the conformational analysis. But since the two low-energy 3′-endo and 2′-endo conformers of the sugar ring display quite different exocyclic vicinal proton coupling constants (Haasnoot et al., 1980, 1981), it is possible to obtain an estimation of sugar ring conformation broadly in terms of N- and S-types, on the basis of $J_{1'2'}$, $J_{1'2''}$, $\sum 2'$, and $\sum 2''$ values. The features of the COSY cross-peaks of all seven residues (except C8 whose H2′ and H2″ peaks overlap) are qualitatively similar. First, large $\sum 1'$ ($\geq$13.3 Hz), small $|J_{1'2'} - J_{1'2''}|$, and $J_{1'2'} > J_{1'2''}$ were observed for all residues. The H2′ and H2″ resonances reflect $\sum 2' > \sum 2''$, and $\sum 3'$ values are small (aside from $^3J_{H3'P}$, the H3′ outer-peak splitting is <20 Hz) in all residues. Unlike observations for several other oligomers (Chazin et al., 1986; Hosur et al., 1986; Suzuki and James, unpublished data) where $J_{2''3'}$ values are so small that 2″–3′

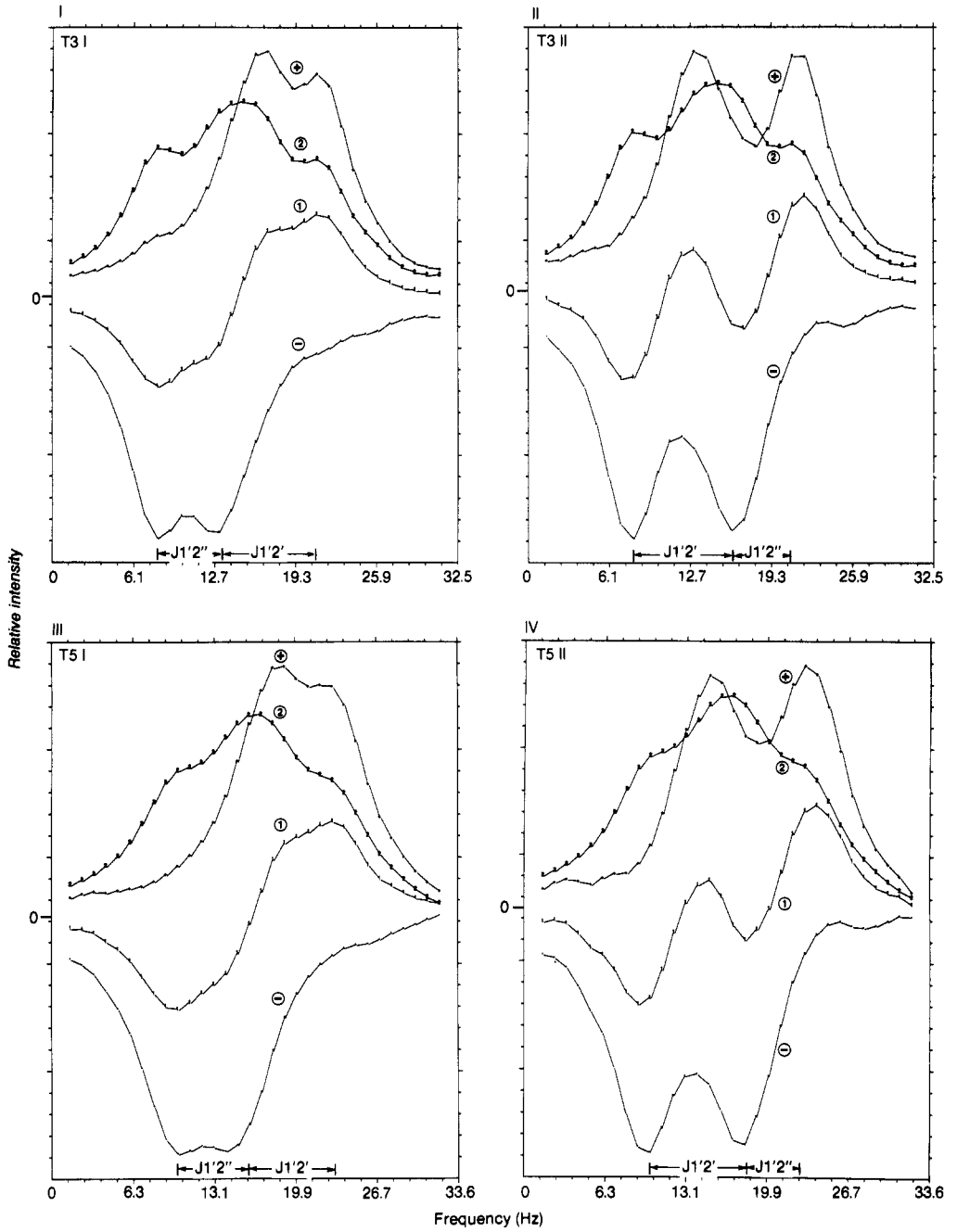

FIGURE 4: DISCO analysis for determination of $J_{1'2'}$ and $J_{1'2''}$. Frames I and II pertain to residue T3 and frames III and IV to T5. In each of frames I and III, trace 1 represents the composite H1′–H2′ cross-peak, and trace 2 represents the composite H1′ diagonal peak (see Materials and Methods for details). Addition and subtraction, respectively, of traces 1 and 2 yield traces marked (+) and (−), from which the $J_{1'2'}$ and $J_{1'2''}$ coupling constants can be extracted as indicated in the figure. Similarly, frames II and IV pertain to the H1′–H2″ cross-peak; from the sum and difference traces, values of $J_{1'2''}$ and $J_{1'2'}$ may also be extracted. In each case, the y axis represents the signal intensity (scaled to cross-peak intensity), and the x axis is in hertz.

cross-peaks were not detected, in the present study the $J_{2''3'}$ of six residues were observed as weak or very weak cross-peaks (Figure 5B). All 3′–4′ cross-peaks were detected. All of these features indicate that the sugar ring conformations are predominantly S-type (2′-endo, 3′-exo, 1′-exo). No obvious sequence dependence of sugar ring conformation was observed in the duplex.

A graphic analysis method suggested by Rinkel and Altona (1987), assuming a C3′-endo, C2′-endo two-state equilibrium, was employed. By use of their analytical model, the pseudorotational phase angle P and maximum ring pucker ϕ_m for the major 2′-endo conformer and its equilibrium population F_s were estimated for the eight residues assuming P and ϕ_m for the minor conformer are 9.0° and 40.0°, respectively. The analysis indicated that the major conformer population of the G and C residues ranged from 70% to 74% and that of the T and A residues ranged from 76% to 86% (Table III). With the experimental resolution of 0.6 Hz for 1D and 1.1 Hz for 2D spectra, the root-mean-square deviation (RMS) (ranging from 0.1 to 0.7) for the calculated sugar ring conformational parameters listed in Table III indicates that these are reasonable descriptions of the sugar rings in the octamer duplex. If observed data were fit with the 2′-endo conformer only, the RMS deviation increased to be in the range of 0.5–1.4, suggesting that a structure composed entirely of 2′-endo deoxyribose rings is inadequate. According to the Rinkel and Altona method of analysis, each sugar ring in the octamer could best be described by rapid converting between 2′-endo and 3′-endo conformations, leading to averaged coupling constant values. In the context of this model the sugar rings of G and C nu-

Table III: Calculated Pseudorotational Parameter P_s (deg), Fraction F_s (%), and Coupling Constants (Hz), both Individual and Summed, for the Predominant C2′-Endo Conformer in the Deoxyribose Rings[a]

residue	P_s (±1°)	F_s (±2%)	$\Sigma 1'$	$J_{1'2'}$	$J_{1'2''}$	$J_{1'2'}-J_{1'2''}$	$\Sigma 2'$	$\Sigma 2''$	$\Sigma 3'$	RMS[b]
G1	155	74	13.8	8.1	5.7	2.4	27.9	23.3		0.7
G2	140	70	13.8	7.8	6.0	1.8	28.4	24.0		0.4
T3	142	76	14.0	8.4	5.6	2.7	28.9	23.4		0.2
A4	136	78	14.2	8.4	5.8	2.5	28.8	23.4		0.7
T5	155	86	14.6	8.6	6.0	2.5	28.8	21.9		0.1
A6	155	85	14.5	8.5	6.0	2.5	28.7	22.0		0.4
C7	128	72	13.9			2.3	29.1	23.4		0.1
C8	128	74	13.9	8.2	5.7	2.5	12.3		15.5	0.1

[a] P_N = 9.0° and ϕ_{mN} = 40.0° were assumed in the graphic analysis (see text), and ϕ_{mS} = 38 ± 1° for the above calculation. [b] RMS is the root-mean-square deviation between the observed coupling constants and those of the two-state model.

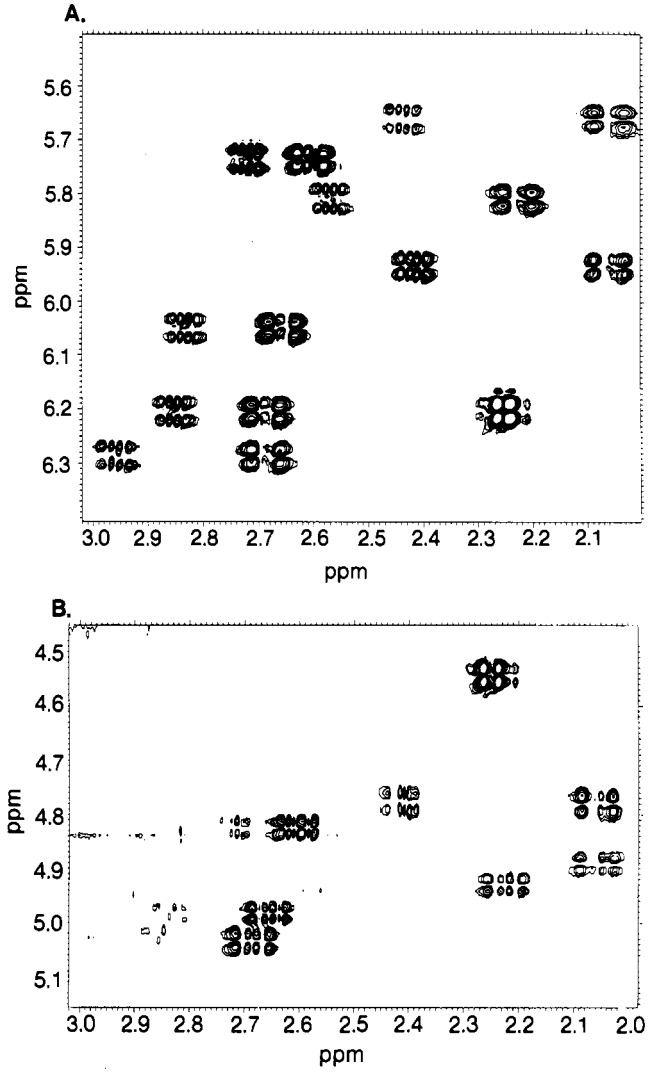

FIGURE 5: Contour plots of the H2′,H2″–H1′ (A) and H2′,H2″–H3′ (B) regions of the phase-sensitive COSY spectrum of [d(GGTATACC)]$_2$, with H2′ and H2″ along the ω_2 dimension.

cleotides exhibit somewhat greater conformational flexibility than T and A, but this does not seem to be related to their location at the octamer termini. An analysis using COSY spectral simulation, considering features of more COSY cross-peaks, may lead to a better description of the sugar ring conformation. Such an analysis could also include consideration of deoxyribose ring descriptions other than the 2′-endo–3′-endo two-state model.

Table IV lists sugar ring pseudorotational parameters for two structural models of [d(GGTATACC)]$_2$ from our previous 2D NOE study (Zhou et al., 1987). With only one structure (or averaged structure), rather than the two-state model examined in the present analysis of vicinal coupling, a somewhat smaller phase angle P than that of the major conformer in the two-state model yields a better fit to ^{1}H–^{1}H NOE data. The parameters listed are more suggestive of the C1′-exo range of S-type conformation. The pseudorotation angles of the single structure, which is in accord with the 2D NOE data, are consistent with a weighted average of the two conformers used in the present coupling constant analysis. That does not necessarily mean the two-state model is correct in detail. Still, we can compare the structural features of the dominant conformer from the two-state model with the 2D NOE results.

Table IV: Deoxyribose Pseudorotational Parameters P (deg) and ϕ_m (deg) for Two Models of [d(GGTATACC)]$_2$[a]

	energy-minimized BDB		energy-minimized B	
residue	P	ϕ_m	P	ϕ_m
G1	153	36	149	41
G2	133	47	147	38
T3	90	40	115	41
A4	188	35	132	39
T5	126	45	131	48
A6	165	37	171	35
C7	124	39	156	39
C8	100	39	105	43

[a] Averaged values from the two complementary strands of the duplex are listed. The two models are discussed in detail by Zhou et al. (1987). The energy-minimized B structure was generated by energy refinement of the standard B-DNA structure with inclusion of all atoms, including hydrogens, and counterions. The energy-minimized BDB model was similarly generated with an initial structure with the GC base pairs in B form and the TATA segment in wrinkled-D form. Nine water molecules were also explicitly included.

The P angles of the GG and CC parts of the energy-minimized BDB model correspond most closely with the results of the present study. The P values of the -TATA- moiety from both models are in the vicinity of C2′-endo and C1′-exo conformation, the same range as those from the present study. But neither model provided a better fit to the experimental data of Table III than the two-state model. The feature of the energy-minimized BDB model that the A residues have larger P values than others was not evident with the present coupling constant analysis. Considering that NOE and exocyclic proton–proton vicinal coupling constants are more sensitive in different ranges of sugar conformation, it is important to combine both NOE and coupling constant data to determine sugar ring conformations.

Conclusions

All cross-peaks from coupled deoxyribose ring protons of [d(GGTATACC)]$_2$ were resolved in phase-sensitive COSY experiments. The qualitative features of cross-peak fine structure were similar for all residues.

Sums of coupling constants, $\Sigma 1'$, $\Sigma 2''$, and $\Sigma 2'$ of all residues and $\Sigma 3'$ of C8, were measured from outer-peak splittings of corresponding cross-peaks along the ω_2 dimension.

Individual $J_{1'2'}$ and $J_{1'2''}$ values could not be measured directly due to partial cancellation of inner peaks of the H1′–H2′ and H1′–H2″ cross-peaks. By taking sums and differences of H1′ diagonal peaks and H1′–H2′ and H1′–H2″ cross-peaks (DISCO procedure), $J_{1'2''}$ and $J_{1'2'}$ were obtained from resulting "decoupled" H1′ signals.

On the basis of an N-type and S-type two-state conformational equilibrium, and Haasnoot's et al. (1980) well-tested, modified Karplus equation for the deoxyribose ring, the pseudorotational parameters P and ϕ_m of the major conformer were calculated for every residue. The S-type deoxyribose ring conformer was predominant, with the relative population ranging from 70% to 86%. The population of the major conformer was higher (76–86%) for A and T nucleotides than for G and C nucleotides (70–74%).

ACKNOWLEDGMENTS

We thank Drs. Vladimir J. Basus and Ruud M. Scheek for help in obtaining the NMR spectra.

Registry No. d(GGTATACC), 80407-93-8; deoxyribose, 533-67-5.

REFERENCES

Altona, C. (1982) *Recl.: J. R. Neth. Chem. Soc. 101*, 413–433.

Altona, C., & Sundaralingam, M. (1972) *J. Am. Chem. Soc. 94*, 8205–8212.

Bermel, W., Kessler, H., Griesinger, C., & Oschkinat, H. (1986) *Bruker Rep. No. 1*, 22–25.

Bodenhausen, G., Kogler, H., & Ernst, R. R. (1984) *J. Magn. Reson. 58*, 370–388.

Boelens, R., Scheek, R. M., Dijkstra, K., & Kaptein, R. (1985) *J. Magn. Reson. 62*, 378–386.

Broido, M. S., Zon, G., & James, T. L. (1984) *Biochem. Biophys. Res. Commun. 119*, 663–670.

Chazin, W. J., Wüthrich, K., Hyberts, S., Rance, M., Denny, W. A., & Leupin, W. (1986) *J. Mol. Biol. 190*, 439–453.

Drew, H. R., & Dickerson, R. E. (1981) *J. Mol. Biol. 151*, 535–556.

Drobny, G., Pines, A., Sinton, S., Weitekamp, D. P., & Wemmer, D. (1979) *Faraday Div. Chem. Soc. Symp. 13*, 49–55.

Griesinger, C., Sorensen, O. W., & Ernst, R. R. (1985) *J. Am. Chem. Soc. 107*, 6394–6396.

Haasnoot, C. A. G., De Leeuw, F. A. A. M., & Altona, C. (1980) *Tetrahedron 36*, 2783–2792.

Haasnoot, C. A. G., De Leeuw, F. A. A. M., De Leeuw, H. P. M., & Altona, C. (1981) *Org. Magn. Reson. 15*, 43–52.

Hosur, R. V., Ravikumar, M., Chary, K. V. R., Sheth, A., Govil, G., Tan, Z. K., & Miles, H. T. (1986) *FEBS 205*, 71–76.

Hoult, D. I., & Richards, R. E. (1975) *Proc. R. Soc. London, A 344*, 311–320.

Jamin, N., James, T. L., & Zon, G. (1985) *Eur. J. Biochem. 152*, 157–166.

Kessler, H., Muller, A., & Oschkinat, H. (1985) *Magn. Reson. Chem. 23*, 844–852.

Kessler, H., Oschkinat, H., & Griesinger, C. (1986) *J. Magn. Reson. 70*, 106–133.

Marion, D., & Wüthrich, K. (1983) *Biochem. Biophys. Res. Commun. 113*, 967–974.

Oschkinat, H., & Freeman, R. (1984) *J. Magn. Reson. 60*, 164–169.

Rinkel, L. J., & Altona, C. (1987) *J. Biomol. Struct. Dyn. 4*, 621–649.

Saenger, W. (1984) *Principles of Nucleic Acid Structure*, Springer, New York.

Scheek, R. M., Russo, N., Boelens, R., & Kaptein, R. (1983) *J. Am. Chem. Soc. 105*, 2914–2916.

Scheek, R. M., Russo, N., Boelens, R., & Kaptein, R. (1984) *Biochemistry 23*, 1371–1376.

States, D. J., Haberkorn, R. A., & Ruben, D. J. (1982) *J. Magn. Reson. 48*, 286–292.

Stejskal, E. O., & Schaefer, J. (1974) *J. Magn. Reson. 14*, 160–169.

Suzuki, E., Pattabiraman, N., Zon, G., & James, T. L. (1986) *Biochemistry 25*, 6854–6865.

Widmer, H., & Wüthrich, K. (1986) *J. Magn. Reson. 70*, 270–279.

Widmer, H., & Wüthrich, K. (1987) *J. Magn. Reson. 74*, 316–336.

Zhou, N., Bianucci, A. M., Pattabiraman, N., & James, T. L. (1987) *Biochemistry 26*, 7905–7913.